Springer

Precision loss of ball screw mechanism under sliding-rolling mixed motion behavior

QI Bao-bao(齐宝宝)[1, 2], CHENG Qiang(程强)[1, 2], LI Shun-lei(李顺磊)[1, 3],
LIU Zhi-feng(刘志峰)[1, 3], YANG Cong-bin(杨聪彬)[1, 3]

1. Institute of Advanced Manufacturing and Intelligent Technology, Beijing University of Technology,
Beijing 100124, China;
2. Beijing Key Laboratory of Advanced Manufacturing Technology, Beijing University of Technology,
Beijing 100124, China;
3. Mechanical Industry Key Laboratory of Heavy Machine Tool Digital Design and Testing,
Beijing University of Technology, Beijing 100124, China

Abstract: The sliding-rolling mixed motion behavior degrades the ball screw's precision at different levels. Based on the sliding-rolling mixed motion between ball and screw/nut raceway, the ball screw's precision loss considering different given axial loading and rotational speed working conditions was investigated. Since creep and lubrication relate to sliding and rolling motion wear, the creep and lubrication characteristics are analyzed under different working conditions. Besides, the precision loss was calculated considering the sole influence of sliding behavior between ball and screw and compared with the results from other current models. Finally, research on precision loss owing to the sliding-rolling mixed motion behavior was realized under given working conditions, and suitable wear tests were carried out. The analytical results of precision loss are in good agreement with the experimental test conclusions, which is conducive to better predicting the law of precision loss in stable wear period.

Key words: ball screw mechanism; precision loss; sliding-rolling mixed motion; creep; lubrication

1 Introduction

As driving functional components, ball screw mechanisms (BSMs) are among the most used components for precision equipment in various fields, such as machine tools [1]. The decline of the BSM precision level can restrict the accuracy level of precision equipment. Precision retention of ball screw refers to the ability to maintain precision at a certain precision level under specified operating conditions and times. However, the sliding-rolling mixed motion behavior influences the ball screw's precision degradation at different degrees. Studies on BSM precision loss include precision degradation basics and analysis of precision degradation, revealing the law of precision degradation.

The basics of the BSM precision degradation include statics, kinematics [2−4], and dynamics [1, 5]. LIN et al [2] proposed the basic kinematic

1358

J. Cent. South Univ. (2021) 28: 1357−1376

analysis method for ball screws. Further, WEI et al [3] improved the ball screws kinematic model based on LIN's model by considering the effect of contact angle and elastic contact deformation on kinematics. The kinematics model [2] was applied to the optimization analysis of BSM transmission efficiency by LIN et al [4], and WEI et al [6] extended the transmission efficiency optimization model of the BSM based on LIN's work. By considering the influence of preload and lubrication on contact kinematics, WEI et al [7] selected the preload-adjustable BSM as the research object. YANG et al [1] and LIU et al [5], respectively, studied the BSM feed dynamics control and dynamic performance optimization. Moreover, CHEN et al [8] established BMS's contact stiffness considering the impact of the contact angle and helix's rise angle on dynamics.

Besides, ZHAO et al [9], ZHEN et al [10], and LIN et al [11] studied the contact load distribution by considering the motion torque and geometric error. KANG [12] designed a series of experiments to detect the BSM friction torque models. Through creep analysis, XU et al [13] proposed a novel ball screw friction torque model. By considering the impact of preload on friction torque, ZHOU et al [14] selected the preload-adjustable BSM as the object of their experimental investigation. Finally, WEI et al [15] and KAMALZADEH et al [16] revealed the effects of preload and elastic deformation on the BSM wear rate.

At present, studies on BSM precision degradation are mainly performed from the perspective of sliding wear. According to the ball screw kinematics analysis results, there are two types of motion in BSM, rolling and sliding [14, 17, 18]. Based on ARCHARD's [19] model, WEI et al [15], ZHOU et al [20], LIU et al [21], CHENG et al [22], and ZHOU et al [23] studied the BMS wear. ZHOU et al [20] and LIU et al [21] studied the screw precision degradation rate in line with wear model, and the BSM precision degradation due to wear result under time-varying working conditions was studied by CHENG et al [22]. The BSMs wear coefficient was obtained by ZHOU et al [23] through design experiments. LIU et al [24] developed a compensation method for thermal error. By detecting the motor current and the vibration signal of BSM, NGUYEN et al [25] realized the preload monitoring. CHENG et al [26] established the attenuation model of machine tool accuracy, considering the decline of transmission components accuracy. Then, CAI et al [27] and CHENG et al [28, 29] described the coordinate transformation relationship between two adjacent bodies in a multi-body system and established an accuracy prediction model for the vertical machining center [30, 31]. Moreover, the research results can be applied to the accuracy prediction of various machine tools.

Despite the progress, the degradation law of the ball screw's positioning precision considering the effects of the sliding-rolling mixed motion behavior has not been studied, as well as the BSM precision degradation and its precision loss rate due to sliding-rolling mixed motion behavior. In order to update the study of precision loss, the BSM sliding-rolling mixed motion behavior considering given axial loading and rotational speed working conditions was studied in this paper. Furthermore, the BSM precision degradation and BSM precision loss rate were also gained in the light of the sliding-rolling mixed motion behavior in this study.

2 Ball screw mechanisms creep rate

Creep analysis is the basis for resolving the problem of the BSM rolling contact, including the BSM rolling friction [13] and the BSM rolling contact wear [32, 33]. This paper uses the BSM coordinate system shown in Figure 1 [13, 22].

O-XYZ is the global coordinate system, and O_b-TNB is the free coordinate system. Both S−$x_s y_s z_s$ and N−$x_n y_n z_n$ are local coordinate systems. For the meaning of other parameters in the figure, refer to the Nomenclature.

The creep rate of ball and nut along the x_n and y_n direction, i.e., ς_{xn} and ς_{yn}, according to KALKER's linear creep [31], is expressed as follows:

$$\varsigma_{xn} = \left(\omega_{b-xn} - \omega_{N-xn} \right) / \omega_{b-N} \tag{1a}$$

$$\varsigma_{yn} = \left(\omega_{b-yn} - \omega_{N-yn} \right) / \omega_{b-N} \tag{1b}$$

where ω_{b-xn} and ω_{b-yn} are the components of ball spin angular velocity ω_{br} in the x_n and y_n directions, respectively. ω_{br} was obtained [34, 35]:

$$\omega_{br} = \frac{-\left(1 + \dfrac{r}{p_{oo_b}} \cos \theta_n \right) \cos \alpha}{\dfrac{r}{p_{oo_b}} \cos \left(\alpha - \theta_n \right)} \tag{2}$$

Therefore, ω_{b-xn} and ω_{b-yn} can be written as:
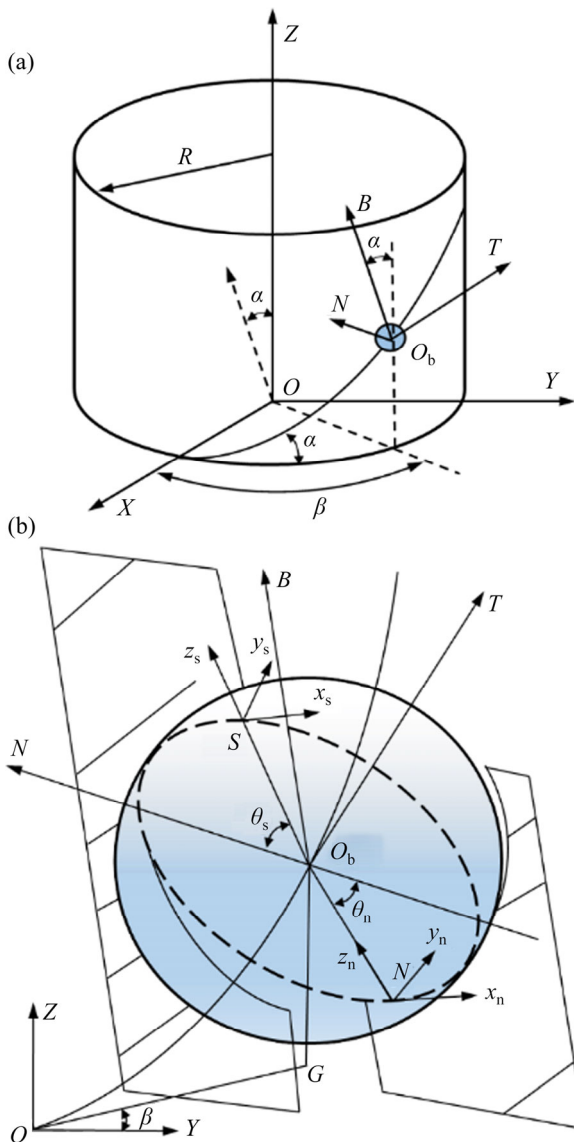
Figure 1 BSM global-contact coordinate system and transformation relationship between coordinates $O\text{-}XYZ$, $O_b\text{-}TNB$, $S\text{-}x_s y_s z_s$ and $N\text{-}x_n y_n z_n$

$$\omega_{b-xn} = (\delta_{ni} - r)(\omega_n \cos\theta_n + \omega_b \sin\theta_n) \tag{3a}$$

$$\omega_{b-yn} = (r - \delta_{ni})/\omega_t \tag{3b}$$

The components ω_{N-xn} and ω_{N-yn} of nut's angular velocity ω_N in the x_n and y_n directions, respectively, are as follows:

$$\omega_{N-xn} = -\omega_N \left[R + (r - \delta_{ni})\cos\theta_n \right] \tag{4a}$$

$$\omega_{N-yn} = 0 \tag{4b}$$

The rolling speed between the ball and nut, ω_{b-N} is:

$$|\omega_{b-N}| = \frac{1}{2}\sqrt{(\omega_{b-xn} + \omega_{b-yn})^2 + (\omega_{N-xn} + \omega_{N-yn})^2} \tag{5}$$

In the equations above, δ_{ni} is the contact

deformation between the i-th ball and the nut, expressed as follows:

$$\delta_{ni} = \chi_{GSni}\left(\frac{9}{16E_{ni}^{\,2} r_n}\right)^{\frac{1}{3}} F_{ni}^{\frac{2}{3}} \tag{6}$$

where χ_{GSni} (see Table 1) is the correction factor in the Hertz contact equation.

Table 1 Initial parameters of BSM

Parameter	Value
Nominal diameter of BSM/mm	50
Ball diameter/mm	6.75
Nut track curvature radius, r_n/mm	3.673
Screw track curvature radius, r_s/mm	3.673
Contact angle/(°)	45
Helix angle/(°)	4.17
Helical pitch/mm	12
Tested length of the screw/mm	300
Axial length of nuts/mm	80
Number of balls	136
Circle's number×column's number	2.5×2
Raceway curvature ratio	0.2725
Hardness of screw or nut (HRC)	62
Hardness of ball (HRC)	63
Elastic modulus/GPa	205
Poisson ratio	0.3
Correction factor (χ_{GSsi}, χ_{GSni})	1
Mean square of ball roughness/μm	2.2
Mean square of screw roughness/μm	2.3
Mean square of nut roughness/μm	2.3
Lubrication mode	Grease
Viscosity of lubricant (25 °C)/(Pa·s)	0.04
Pressure-viscosity coefficient/(m²·N⁻¹)	2.2×10^{-8}
Temperature-viscosity coefficient/K⁻¹	4.7×10^{-3}
Boundary wear coefficient, K_{bl}	3.2×10^{-11}

ω_n, ω_b and ω_t are given as:

$$\omega_n = -\omega_{br}\sin\varphi \tag{7a}$$

$$\omega_b = -\omega_{br}\cos\varphi\cos\vartheta \tag{7b}$$

$$\omega_t = \omega_{br}\cos\varphi\sin\vartheta \tag{7c}$$

ω_N is nut's angular velocity, expressed as:

$$\omega_N = -\omega\left(\frac{R}{\cos\alpha} + r\cos\theta_s\cos\alpha\right) \tag{8}$$

ς_{xn} and ς_{yn} are expressed as:

$$\varsigma_{xn} = 2\left\{\left[(r-\delta_{ni})\left[\omega_{br}(\sin\varphi\cos\theta_n + \cos\varphi\cos\vartheta\sin\theta_n) + \right.\right.\right.$$

$$\left.\omega\cos\theta_n\left(\frac{R}{\cos\alpha} + r\cos\theta_s\cos\alpha\right)\right] + \omega_N R\right]\Big/$$

$$\left[\omega_N R + (r-\delta_{ni})(\omega_{br}\cos\varphi\cos\vartheta\cos\theta_n + \right.$$

$$\left.\left.\omega_{br}\sin\varphi\sin\theta_n + \omega_N\cos\theta_n)\right]\right\} \tag{9a}$$

$$\varsigma_{yn} = 2\left\{\left[(r-\delta_{ni}) + \omega_{br}\cos\varphi\sin\vartheta\right]\Big/ \right.$$

$$\left[\omega_N R + (r-\delta_{ni})(\omega_{br}\cos\varphi\cos\vartheta\cos\theta_n + \right.$$

$$\left.\left.\omega_{br}\sin\varphi\sin\theta_n + \omega_N\cos\theta_n)\right]\right\} \tag{9b}$$

Similarly, based on Ref. [33], the creep rates between the ball and screw in the x_s and y_s directions, ς_{xs} and ς_{ys}, are expressed as:

$$\varsigma_{xs} = (\omega_{b-xs} - \omega_{S-xs})/\omega_{b-S} \tag{10a}$$

$$\varsigma_{ys} = (\omega_{b-ys} - \omega_{S-ys})/\omega_{b-S} \tag{10b}$$

where ω_{b-S} is the rolling speed between the ball and screw, given by

$$\omega_{b-S} = \frac{1}{2}\left[\omega R + (r-\delta_{si})(\omega_n\cos\theta_s + \omega_b\sin\theta_s - \omega\cos\theta_s)\right] \tag{11}$$

The angular velocity components of ball or screw in the x_s and y_s directions, namely ω_{b-xs}, ω_{b-ys} or ω_{S-xs}, ω_{S-ys}, can be calculated as:

$$\omega_{b-xs} = (\delta_{si} - r)(\omega_n\cos\theta_s + \omega_b\sin\theta_s) \tag{12a}$$

$$\omega_{b-ys} = (\delta_{si} - r)\omega_t \tag{12b}$$

$$\omega_{S-xs} = \omega\left[(r-\delta_{si})\cos\theta_s - R\right] \tag{13a}$$

$$\omega_{S-ys} = 0 \tag{13b}$$

where δ_{si} is the contact deformation between the i-th ball and the screw, expressed as:

$$\delta_{si} = \chi_{GSsi}\left(\frac{9}{16E_{si}^2 r_s}\right)^{\frac{1}{3}} F_{si}^{\frac{2}{3}} \tag{14}$$

where r_s is is the track curvature radii of the screw.

Finally, ς_{xs} and ς_{ys} are expressed as:

$$\varsigma_{xs} = [2(\delta_{si} - r)(\omega\cos\theta_s - \omega_{br}\sin\varphi\cos\theta_s - \omega_{br}\cos\varphi\cos\vartheta\sin\theta_s) + \omega R]/[\omega R + (r-\delta_{si})(\omega_n\cos\theta_s + \omega_b\sin\theta_s - \omega\cos\theta_s)] \tag{15a}$$

$$\varsigma_{ys} = \frac{2(\delta_{si} - r)\omega_{br}\cos\varphi\sin\vartheta}{\omega R + (r-\delta_{si})(\omega_n\cos\theta_s + \omega_b\sin\theta_s - \omega\cos\theta_s)} \tag{15b}$$

3 Ball screw mechanisms lubrication analysis

The lubricant film thickness and contact surface roughness have diverse degrees of influence on the wear coefficient [36]. Figure 2 shows the BSM lubrication analysis diagram.

According to Ref. [7], the lubricant film thickness between the ball and the raceway h_{b-k} can be written as follows:

$$h_{b-k} = h_{cb-k} + \frac{i_k^2}{2R_1} + \frac{j_k^2}{2R_2} + e_{b-k}(i_k, j_k) - e_{b-k}(0,0) \tag{16}$$

where h_{cb-k} ($k=s$ or n) is the contact center lubricant thickness between the ball and screw or the nut that can be obtained from Ref. [35]. R_1 or R_2 is the
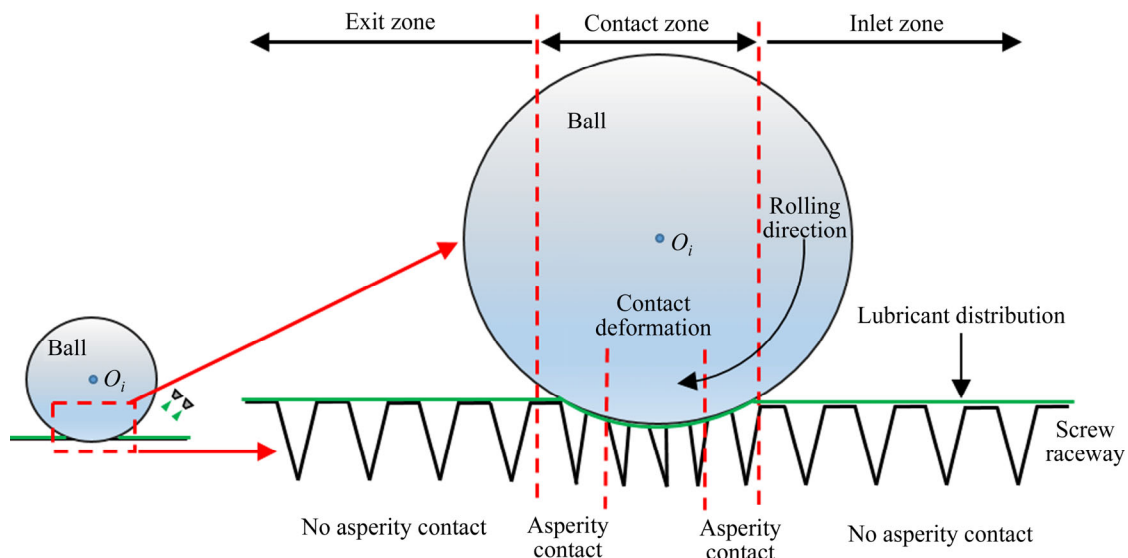

Figure 2 Lubricated contact status between ball and raceway

curvature sum of ball and screw or ball and nut, and $e_{b-k}(i_k, j_k)$ is the elastic deformation of ball and screw and that of ball and nut [37].

$$h_{cb-s} = 2.385 U_{b-s}^{0.7} G_{b-s}^{0.46} W_{b-s}^{-0.09} \cdot$$
$$\left[d_b \left(D_s - d_b \cos\theta_s \right) \right] / \left[D_s - d_b \cos\theta_s \left(1 - \cos\alpha \right) \right]$$
$$(17a)$$

$$h_{cb-n} = 2.385 U_{b-n}^{0.7} G_{b-n}^{0.46} W_{b-n}^{-0.09} \cdot$$
$$\left[d_b \left(D_n + d_b \cos\theta_n \right) \right] / \left[D_n - d_b \cos\theta_n \left(1 - \cos\alpha \right) \right]$$
$$(17b)$$

$$\frac{1}{R_1} = \frac{1}{r_b} + \frac{1}{D_s/2} \tag{18}$$

$$\frac{1}{R_2} = \frac{1}{r_b} - \frac{1}{D_n/2} \tag{19}$$

where U_{b-s} and U_{b-n} are the dimensionless velocity between the ball and screw and that between the ball and nut [34]; G_{b-s} and G_{b-n} are the BSM material parameters and relate to the pressure-viscosity coefficient of lubricant, γ; W_{b-s} and W_{b-n} are dimensionless contact loading; D_s and D_n are the inner diameter of screw and that of the nut, respectively; E^* is the equivalent elastic modulus of the ball and the raceway.

$$U_{b-s} = \frac{\eta_{vs} u_{b-s}}{E^* R_1} \tag{20a}$$

$$U_{b-n} = \frac{\eta_{vn} u_{b-n}}{E^* R_2} \tag{20b}$$

$$G_{b-s} = G_{b-n} = \gamma E^* \tag{21}$$

$$W_{b-s} = \frac{P_{si}}{E^* R_1^2} \tag{22a}$$

$$W_{b-n} = \frac{P_{ni}}{E^* R_2^2} \tag{22b}$$

$$\frac{1}{E^*} = \frac{1}{2} \left(\frac{1-v_1^2}{E_1} + \frac{1-v_2^2}{E_2} \right) \tag{23}$$

where η_{vs} and η_{vn} are the lubricant's dynamic viscosity. The relationship between viscosity, pressure, and temperature is as follows[38]:

$$\eta_{vs}(F_{si}, T_s) = \eta_{vs,0} \exp\left[\gamma F_{si} - \lambda (T_s - T_{vs,0}) \right] \tag{24a}$$

$$\eta_{vn}(F_{ni}, T_n) = \eta_{vn,0} \exp\left[\gamma F_{ni} - \lambda (T_n - T_{vn,0}) \right] \tag{24b}$$

where $\eta_{vs,0}$ is the lubricant's viscosity at temperature $T_{vs,0}$; $\eta_{vn,0}$ is the lubricant's viscosity at temperature $T_{vn,0}$; γ/λ is the pressure-viscosity coefficient of lubricant (Table 1); λ is the temperature-viscosity coefficient of lubricant (Table 1); F_{si} and F_{ni} are contact loadings between the i-th ball and screw and nut, respectively.

Moreover, u_{b-s} and u_{b-n} are the average sliding velocity in $S-x_s y_s z_s$ and $N-x_n y_n z_n$, respectively:

$$u_{b-s} = \frac{1}{2} \sqrt{ \left(v_{b-xs} + v_{s-xs} \right)^2 + \left(v_{b-ys} + v_{s-ys} \right)^2 } \tag{25a}$$

$$u_{b-n} = \frac{1}{2} \sqrt{ \left(v_{b-xn} + v_{n-xn} \right)^2 + \left(v_{b-yn} + v_{n-yn} \right)^2 } \tag{25b}$$

where v_{b-xs} and v_{b-ys} are the components of the ball velocity in the x_s and y_s direction, respectively; v_{s-xs} and v_{s-ys} are the components of the screw speed in the x_s and y_s directions, respectively; v_{b-xn} and v_{b-yn} are the components of the ball velocity in the x_n and y_n directions, respectively; v_{n-xn} and v_{n-yn} are the components of the nut speed in the x_n and y_n directions, respectively. These terms are expressed as follows:

$$v_{b-xs} = v_{b-s} + \omega_n r \sin\theta_s - \omega_b r \cos\theta_s \tag{26a}$$

$$v_{b-ys} = -\omega_t r \sin\theta_s \tag{26b}$$

$$v_{b-xn} = v_{b-s} - \omega_n r \sin\theta_n + \omega_b r \cos\theta_n \tag{27a}$$

$$v_{b-yn} = -\omega_t r \sin\theta_n \tag{27b}$$

$$v_{s-xs} = r\omega \cos\theta_s \sin(W + \beta) +$$
$$r\omega \sin\theta_s \sin\alpha \cos(W + \beta) - R\omega \sin(W + \beta) \tag{28a}$$

$$v_{s-ys} = -r\omega \cos\theta_s \cos(W + \beta) +$$
$$r\omega \sin\theta_s \sin\alpha \sin(W + \beta) + R\omega \cos(W + \beta) \tag{28b}$$

$$v_{n-xn} = -r\omega \cos\theta_n \sin(W + \beta) -$$
$$r\omega \sin\theta_n \sin\alpha \cos(W + \beta) - R\omega \sin(W + \beta) \tag{29a}$$

$$v_{n-yn} = r\omega \cos\theta_n \cos(W + \beta) -$$
$$r\omega \sin\theta_n \sin\alpha \sin(W + \beta) + R\omega \cos(W + \beta) \tag{29b}$$

In the above equations, the term v_{b-s} is ball's rotational speed relative to screw in the helical direction [3], given by

$$v_{b-s} = \omega_n r \sin\theta_n - \omega_b r \cos\theta_n -$$
$$\omega \left(\frac{R}{\cos\alpha} + r \cos\theta_n \cos\alpha \right) \tag{30}$$

By combining Eqs. (16a)−(18b), the minimum lubricant film thickness h_{minb-s} and h_{minb-n} can be written as:

$$h_{minb-s} = R_1 h_{cb-s} \tag{31a}$$

$$h_{\min b-n} = R_2 h_{cb-n} \tag{31b}$$

In line with the minimum lubricant thickness and the mean square roughness of contact surface, this study introduced the parameter Φ to describe the BSM lubrication state as follows:

$$\Phi = \frac{h_{\min}}{\sqrt{\sigma_b^2 + \sigma_l^2}} \tag{32}$$

where σ_b and σ_l are the mean-square roughness values of the ball and the raceway, respectively. When $h_{\min}=h_{\min b-s}$ and $\sigma_l=\sigma_s$, Eq. (32) expresses the lubrication parameter of ball and screw; when $h_{\min}=h_{\min b-n}$ and $\sigma_l=\sigma_n$, Eq. (32) is the lubrication parameter of the ball and nut.

The roughness morphology and profile heights of the raceways and balls can be obtained through three-dimensional surface topography technique using a three-dimensional topography signal instrument. Figure 3 shows the measured micro-morphology signal of the screw raceway, and Table 1 summarizes the mean-square value of the roughness. This paper assumes that the screw

Figure 3 Three-dimensional micro-morphology signal of screw raceway: (a) 3D rough surface micro-morphology of screw raceway; (b) Profile height along y-direction of 3D rough surface micro-morphology

raceway and nut raceway have the same roughness value. Similarly, the mean square roughness value of the ball was also obtained.

The relationship between the BSM wear coefficient k_d and lubrication parameter Φ is as follows [37]:

$$k_d = \begin{cases} k_{bl}, & \Phi < 1/2 \\ \dfrac{2}{7}k_{bl}(4-\Phi), & 1/2 \le \Phi < 4 \\ 0, & \Phi \ge 4 \end{cases} \tag{33}$$

where k_{bl} is the BSM wear coefficient under the boundary lubrication state (see Table 1).

4 Precision degradation calculation

According to the mixed motion analysis, this study calculates the BSM precision degradation for the sliding and rolling motion separately.

4.1 Precision degradation due to sliding motion wear

According to the Archard model [19], the sliding wear amount can be expressed as follows:

$$V_{sw}(t) = C_{b-s}V_{b-s}(n) + C_{b-n}V_{b-n}(n) \tag{34}$$

where C_{b-s} and C_{b-n} are the total cycles of the ball and screw, and the ball and nut, respectively; $V_{b-s}(n)$ and $V_{b-n}(n)$ are the wear amount of the ball and screw, and the ball and nut, respectively, in one cycle.

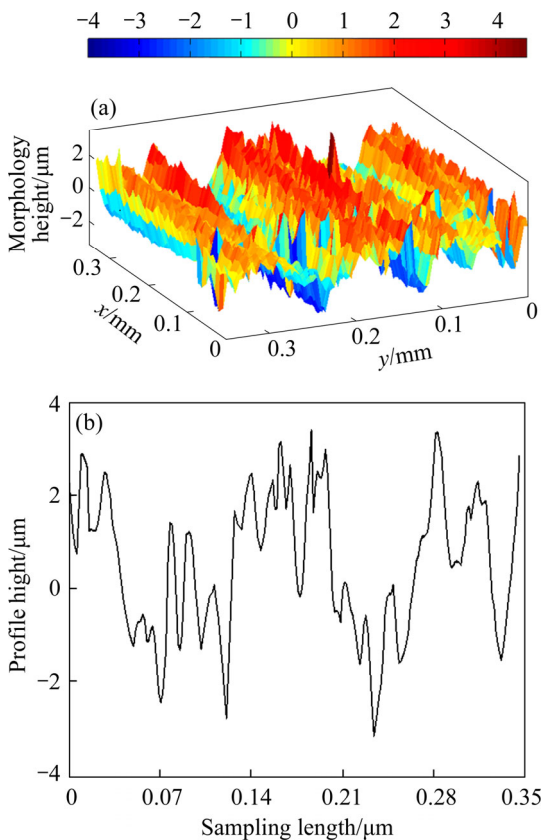$$V_{b-s}(n) = V_{b-s}^1(t) + V_{b-s}^2(t) + \cdots + V_{b-s}^i(t) + \cdots + V_{b-s}^M(t) \tag{35a}$$

$$V_{b-n}(n) = V_{b-n}^1(t) + V_{b-n}^2(t) + \cdots + V_{b-n}^i(t) + \cdots + V_{b-n}^M(t) \tag{35b}$$

where $V^1_{b-s}(t)$ and $V^1_{b-n}(t)$ are the wear amount of the first ball and screw and that of the first ball and nut during one cycle.

$$V_{b-s}^1(t) = V_{b-s1}(t_{ss1}) + V_{b-s2}(t_{ss2}) + \cdots + V_{b-si}(t_{ssi}) + \cdots + V_{b-sM}(t_{ssM}) \tag{36a}$$

$$V_{b-n}^1(t) = V_{b-n1}(t_{ns1}) + V_{b-n2}(t_{ns2}) + \cdots + V_{b-ni}(t_{nsi}) + \cdots + V_{b-nM}(t_{nsM}) \tag{36b}$$

where $V_{b-s1}(t_{ss1})$, $\cdots$, $V_{b-sM}(t_{ssM})$ are the wear amounts of ball and screw from t_{ss1} to t_{ss2}, from t_{ssi} to t_{ssi+1} and from t_{ssM} to t_{ss1} in Eq. (37a); $V_{b-n1}(t_{ns1}),\cdots,V_{b-nM}(t_{nsM})$ are the wear amounts of ball and nut from t_{ns1} to t_{ns2}, from t_{nsi} to t_{nsi+1} and from t_{nsM} to t_{ns1} in Eq. (37b):

$$\begin{cases} V_{\text{b-s1}}(t_{\text{ss1}}) = \int_{t_{\text{ss1}}}^{t_{\text{ss2}}} v_{\text{b-s1}}(t_{\text{ss1}})\,\mathrm{d}t = \\ \qquad \int_{t_{\text{ss1}}}^{t_{\text{ss2}}} K_{\text{b-s}} \dfrac{F_{\text{s1}}}{H_{\text{b-s}}} l_{\text{ss-bs1}}\,\mathrm{d}t \\ \qquad\qquad \vdots \\ V_{\text{b-sM}}(t_{\text{ssM}}) = \int_{t_{\text{ssM}}}^{t_{\text{ss1}}} v_{\text{b-sM}}(t_{\text{ssM}})\,\mathrm{d}t = \\ \qquad \int_{t_{\text{ssM}}}^{t_{\text{ss1}}} K_{\text{b-s}} \dfrac{F_{\text{sM}}}{H_{\text{b-s}}} l_{\text{ss-bsM}}\,\mathrm{d}t \end{cases} \tag{37a}$$

$$\begin{cases} V_{\text{b-n1}}(t_{\text{ns1}}) = \int_{t_{\text{ns1}}}^{t_{\text{ns2}}} v_{\text{b-n1}}(t_{\text{ns1}})\,\mathrm{d}t = \\ \qquad \int_{t_{\text{ns1}}}^{t_{\text{ns2}}} K_{\text{b-n}} \dfrac{F_{\text{n1}}}{H_{\text{b-n}}} l_{\text{nn-bn1}}\,\mathrm{d}t \\ \qquad\qquad \vdots \\ V_{\text{b-nM}}(t_{\text{nsM}}) = \int_{t_{\text{nsM}}}^{t_{\text{ns1}}} v_{\text{b-nM}}(t_{\text{nsM}})\,\mathrm{d}t = \\ \qquad \int_{t_{\text{nsM}}}^{t_{\text{ns1}}} K_{\text{b-n}} \dfrac{F_{\text{nM}}}{H_{\text{b-n}}} l_{\text{nn-bnM}}\,\mathrm{d}t \end{cases} \tag{37b}$$

where $v_{\text{b-s1}}(t_{\text{ss1}}),\ \cdots,\ v_{\text{b-sM}}(t_{\text{ssM}})/v_{\text{b-n1}}(t_{\text{ns1}}),\ \cdots,$ $v_{\text{b-nM}}(t_{\text{nsM}})$ are the wear amounts of ball and screw/nut at $t_{\text{ss1}}, \cdots t_{\text{ss}i} \cdots t_{\text{ssM}}/t_{\text{ns1}}, \cdots t_{\text{ns}i} \cdots t_{\text{nsM}}$ in Eqs. (38a) and (38b). And $F_{\text{s1}}, \cdots, F_{\text{s}i} \cdots, F_{\text{sM}}/F_{\text{n1}}, \cdots F_{\text{n}i} \cdots F_{\text{nM}}$ are the contact loadings of each ball and screw/nut.

$$\begin{cases} v_{\text{b-s1}}(t_{\text{ss1}}) = K_{\text{b-s}} \dfrac{F_{\text{s1}}}{H_{\text{b-s}}} l_{\text{ss-bs}i} \\ \qquad\qquad \vdots \\ v_{\text{b-sM}}(t_{\text{ssM}}) = K_{\text{b-s}} \dfrac{F_{\text{sM}}}{H_{\text{b-s}}} l_{\text{ss-bsM}} \end{cases} \tag{38a}$$

$$\begin{cases} v_{\text{b-n1}}(t_{\text{ns1}}) = K_{\text{b-n}} \dfrac{F_{\text{n1}}}{H_{\text{b-n}}} l_{\text{nn-bn}i} \\ \qquad\qquad \vdots \\ v_{\text{b-nM}}(t_{\text{nsM}}) = K_{\text{b-n}} \dfrac{F_{\text{nM}}}{H_{\text{b-n}}} l_{\text{nn-bnM}} \end{cases} \tag{38b}$$

where $l_{\text{ss-bs1}},\ l_{\text{ss-bs2}},\ \cdots,\ l_{\text{ss-bsM}}$ and $l_{\text{nn-bn1}},$ $l_{\text{nn-bn2}},\ \cdots,\ l_{\text{nn-bnM}}$ are the screw and nut sliding distances relative to the 1st, 2nd, $\cdots$, M-th ball. By taking the i-th ball as an example, one obtains:

$$l_{\text{ss-bs}i} = \frac{R_{\text{bs}i}\,\omega_{si-\text{b}}\,r\cos\alpha}{\pi(1+R_{\text{bs}i})\,v_{\text{bs-ss}i}\,R} \sqrt{R^2 + \left(\frac{L}{2\pi}\right)^2} \cdot$$
$$\sqrt{(R - r\cos\theta_{si})^2 + \left(\frac{L}{2\pi}\right)^2} \tag{39a}$$

$$l_{\text{nn-bn}i} = \frac{R_{\text{bn}i}\,\omega_{ni-\text{b}}\,r\cos\alpha}{\pi(1+R_{\text{bn}i})\,v_{\text{bn-sn}i}\,R} \sqrt{R^2 + \left(\frac{L}{2\pi}\right)^2} \cdot$$
$$\sqrt{(R - r\cos\theta_{ni})^2 + \left(\frac{L}{2\pi}\right)^2} \tag{39b}$$

where $R_{\text{bs}i}$ and $R_{\text{bn}i}$ are the sliding-to-rolling ratios of the i-th ball and screw, and that of the i-th ball and nut, respectively. Based on Ref. [22], $R_{\text{bs}i}$ and $R_{\text{bn}i}$ can be calculated:

$$R_{\text{bs}} = \left[2\left|\omega_n r(\sin\theta_s + \sin\theta_n) - \omega_b r(\cos\theta_n + \cos\theta_s) - \right.\right.$$
$$\left.\omega\left(\frac{R}{\cos\alpha} + r\cos\alpha\cos\theta_n\right)\right|\Big/\left[\left|\omega_n r(\sin\theta_s + \sin\theta_n) - \right.\right.$$
$$\omega_b r(\cos\theta_n + \cos\theta_s) + \omega R\left(\cos\alpha - \frac{1}{\cos\alpha}\right) -$$
$$\omega r\cos\alpha(\cos\theta_s + \cos\theta_n)\Big| + \left|\omega\cos\alpha(R - r\cos\theta_s)\right|\Big] \tag{40}$$

$$R_{\text{bn}} = \left[2\left|\omega_b r(\cos\theta_s + \cos\theta_n) - \omega_n r(\sin\theta_s + \sin\theta_n) + \right.\right.$$
$$\left.\omega\left(\frac{R}{\cos\alpha} + r\cos\alpha\cos\theta_n\right)\right|\Big/\left[\left|\omega_b r(\cos\theta_s + \cos\theta_n) - \right.\right.$$
$$\omega_n r(\sin\theta_s + \sin\theta_n)\Big| + \left|-\omega\left(\frac{R}{\cos\alpha} + r\cos\alpha\cos\theta_n\right)\right|\Big] \tag{41}$$

By combining Eqs. (37a)−(41), one can calculate $V_{\text{b-s}}^2(t),\ \cdots,\ V_{\text{b-s}}^i(t),\ \cdots,\ V_{\text{b-s}}^M(t)$ and $V_{\text{b-n}}^2(t),\ \cdots,\ V_{\text{b-n}}^i(t),\ \cdots,\ V_{\text{b-n}}^M(t)$. Moreover, the sliding wear amount is obtained by bringing Eqs. (36a) and (36b) into Eqs. (35a), (35b) and (34). Based on Eqs. (34) and (36b), the sliding wear depth of ball and screw/nut is given as:

$$h_{\text{sbs}}(n) = \frac{C_{\text{b-s}}(n)V_{\text{b-s}}(n)}{\pi a_{\text{bs}} b_{\text{bs}} L_{\text{b-s}}} A_r \tag{42a}$$

$$h_{\text{sbn}}(n) = \frac{C_{\text{b-n}}(n)V_{\text{b-n}}(n)}{\pi a_{\text{bn}} b_{\text{bn}} L_{\text{b-n}}} A_r \tag{42b}$$

where $h_{\text{sbs}}(n)$ and $h_{\text{sbn}}(n)$ are the screw raceway length and that of nut raceway; a_{bs} is the contact surface long half axes of ball and screw, and b_{bs} is the contact surface short half axes of ball and screw; a_{bn} is the contact surface long half axes of ball and nut; b_{bn} is the contact surface short half axes of ball and nut. The length of the raceway of the screw is $L_{\text{b-s}} = L_s/\sin\alpha$, and the length of the raceway of the nut is $L_{\text{b-n}} = L_n/\sin\alpha$.

According to Refs. [21, 39], the contact area can be established:

$$\begin{cases} \pi a_k b_k = \pi \left(\dfrac{6 N_H R_k P_k}{\pi E^*} \right)^{2/3} \\[2em] A_r = \left[\dfrac{\left(\dfrac{4}{\pi E^*} \dfrac{r_s r}{r_s - r} \right)^{\left(\frac{1}{r} - \frac{1}{r_s} \right)}}{\pi (r_s - r)} \right] \dfrac{D_f}{2 - D_f} a_{Ls} \end{cases} \tag{43}$$

When $k=s$, Eq. (43) gives the contact area of ball and screw; when $k=n$, Eq. (43) gives the contact area of the ball and nut.

The calculation of contact loading was demonstrated. MEI et al [40] established the calculation model for the BSM contact loading. ZHAO et al [9], ZHEN et al [10], and LIN et al [11] studied the contact load distribution by considering the motion torque and geometric error. By considering the preload, WEI et al [7] pointed out the contact state between ball and raceway under different preloads; furthermore, based on the contact state, LI et al [41] conceptualized the correlation among contact loading, axial loading, and preload. Based on Refs. [40], [7] and [41], this paper calculates the contact loading between the ball and screw/nut considering the preload attenuation.

According to Refs. [7, 41], the contact state between ball and raceway can be represented as shown in Figure 4. In Figure 4(a), the axial loading is higher than 2.83 times of preload; in Figure 4(b), the axial loading is lower than 2.83 times of preload. When the axial loading almost equals the preload, BSM is not suitable for precision transmission [7]. Therefore, the study does not discuss this situation.

In Figure 4(a), F_{1a} is the total contact loading among balls, screw, and nut 1 raceway; F_{2a} is the total contact loading among balls, screw, and nut 2 raceway, and they can be written as follows:

$$\begin{cases} F_{1a} + F_{2a} = F_a \\ \left(F_p^{L1}(t) + F_a^{L1} \right)^{\frac{2}{3}} + \left(F_p^{R1}(t) - F_a^{R1} \right)^{\frac{2}{3}} = 2 \left(F_p^{L1}(t) \right)^{\frac{2}{3}} \end{cases} \tag{44}$$

Similarly, F_{1a} and F_{2a} in Figure 4(b) are:

$$\begin{cases} F_{1a} + F_{2a} = F_a \\ \left(F_p^{L2}(t) + F_a^{L2} \right)^{\frac{2}{3}} - \left(F_p^{L2}(t) \right)^{\frac{2}{3}} = \left(F_p^{R2}(t) \right)^{\frac{2}{3}} + \\ \qquad \left(F_a^{R2} - F_p^{R2}(t) \right)^{\frac{2}{3}} \end{cases} \tag{45}$$

According to Ref. [40], F_{si} and F_{ni} ($i=1, \cdots, M$) can be obtained as:
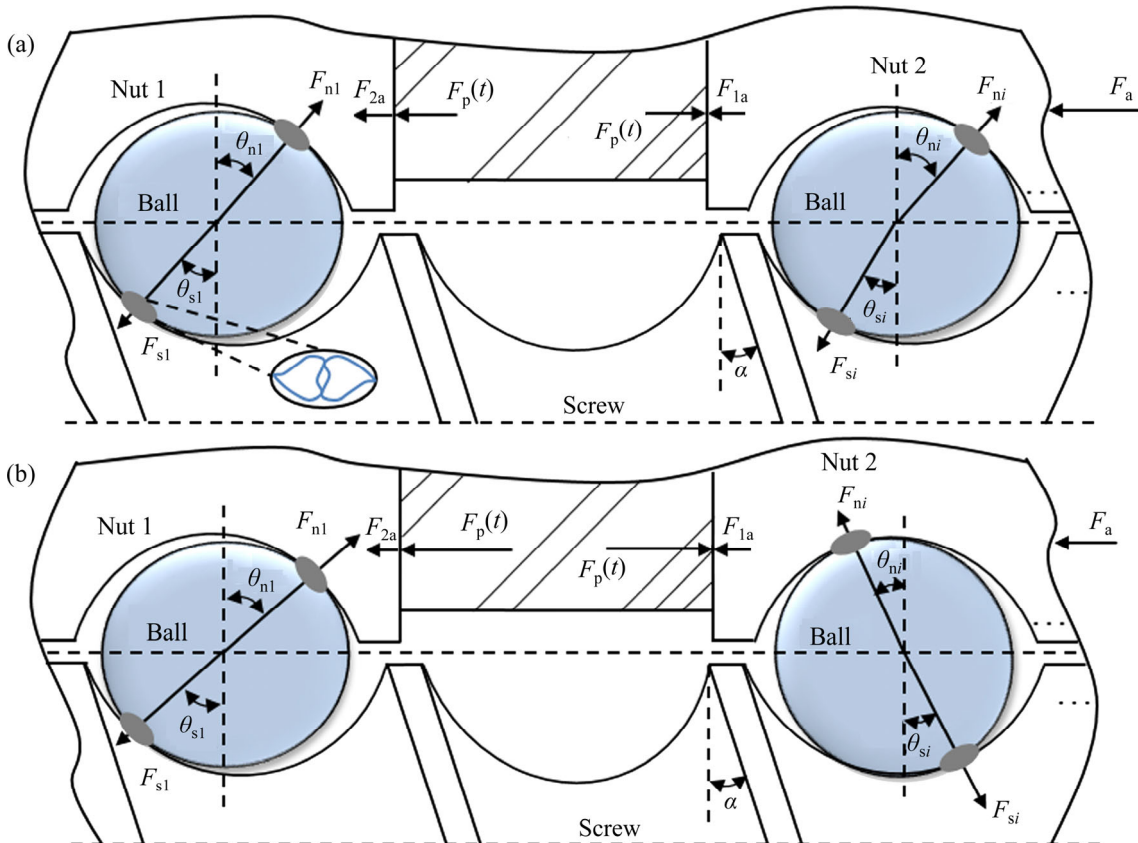
Figure 4 Contact state: (a) Axial loading is greater than 2.83 times of preload; (b) Axial loading is smaller than 2.83 times of preload

$$F_{si} = F_{m} - \sum_{j=1}^{i-1} P_{sj} \sin\theta_{sj} \cos\alpha \qquad (46a)$$

$$F_{ni} = F_{m} - \sum_{j=1}^{i-1} P_{nj} \sin\theta_{nj} \cos\alpha \qquad (46b)$$

where $F_{p}(t)$ can be obtained from Ref. [42]. In contact state in Figure 4(a), when the ball contacts nut 1, $F_{m} = F_{1a} + F_{p}(t)$; when the ball contacts nut 2, $F_{m} = F_{2a} - F_{p}(t)$. In contact state in Figure 4(b), when the ball contacts nut 1, $F_{m} = F_{1a} + F_{p}(t)$; when the ball contacts with nut 2, $F_{m} = F_{p}(t) - F_{2a}$. For the detailed calculations, refer to Refs. [40, 7, 41, 42].

4.2 Precision degradation due to rolling motion wear

In the rolling motion contact area of ball and raceway, there are partial sliding and partial adhesion phenomena [32, 33]. Figure 5 shows a schematic of rolling motion contact of ball and screw/nut raceways.

Based on Ref. [32], the rolling wear depth of single ball and screw is deduced:

$$\Delta h_{rbs} = k_{bs} \frac{F_{si}}{A(\varsigma)} v_{rbs} \Delta t \qquad (47)$$

where k_{bs} is the dimension wear coefficient, $k_{bs} = k_{d}/H_{b-s}$; according to Eq. (44), $A(\varsigma) \approx a_{k}b_{k}/9$; v_{rbs} is the creep velocity.

At time t_i, the wear depth is given owing to rolling motion as:

$$h_{rbs} = h_{rbs}(t_{i-1}) + k_{bs} \frac{F_{si}}{A(\varsigma_{xs})} \left\| S_{bs}(t_i) - S_{bs}(t_{i-1}) \right\| \qquad (48)$$

where S_{bs} is the creep value in rolling motion contact.

By combining Eqs. (47) and (48), the accumulative wear depth owing to rolling motion behavior in the x_s direction can be obtained:

$$h_{rbs}^{xs} = h_{rbs}^{xs}(t_A^{xs}) + \int_{t_A^{xs}}^{t_i^{xs}} k_{bs} \frac{F_{si}}{A(\varsigma_{xs})} v_{rbs}^{xs} dt_i^{xs}, \quad t_i^{xs} < t_C^{xs} \qquad (49)$$

where v_{rbs}^{xs} is the sliding velocity between ball and screw in the x_s direction given by:

$$v_{rbs}^{xs} = v_{b-s}^{xs} \varsigma_{xs} \qquad (50)$$

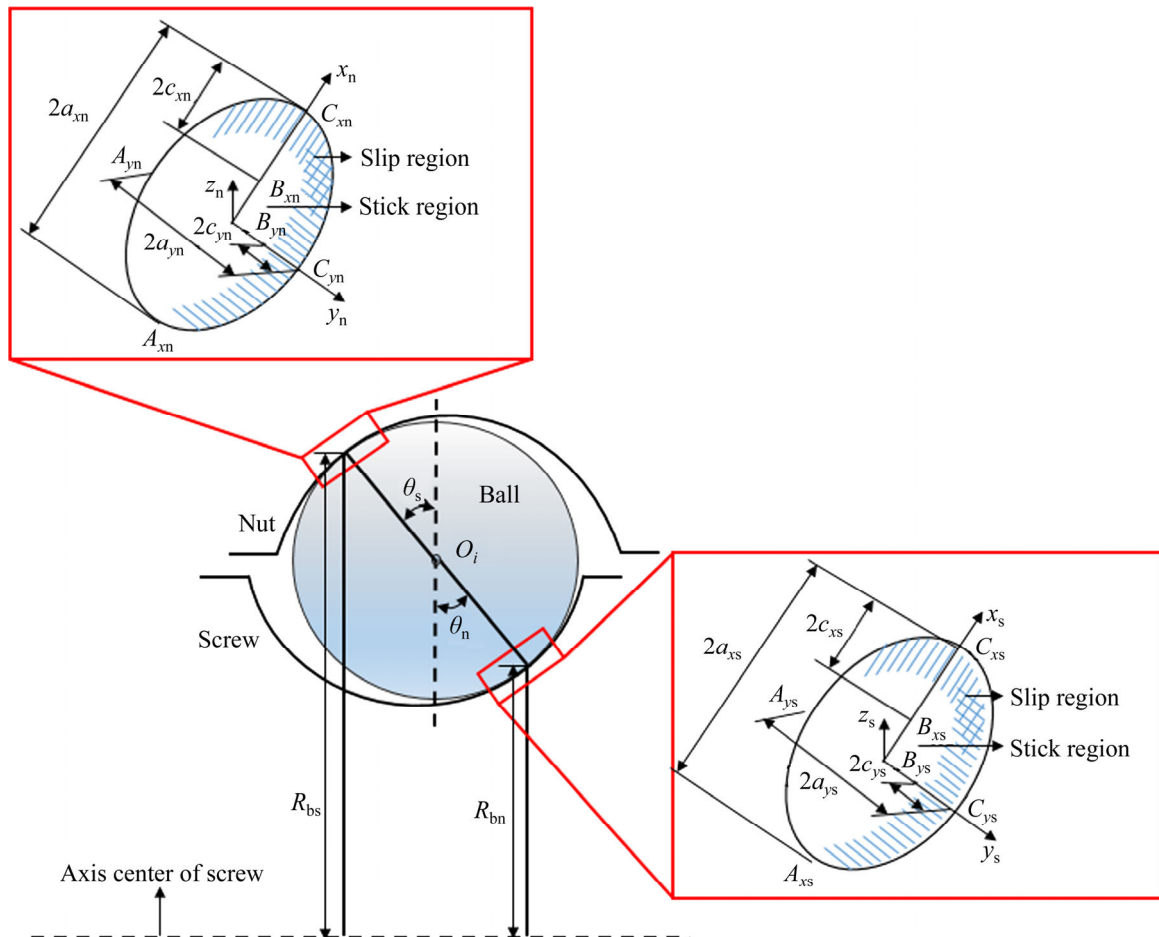In Eq. (50), v_{b-s}^{xs} is the average rolling velocity

Figure 5 Rolling motion contact of ball and screw/nut raceway: Partial slip and partial stick regions

1366

J. Cent. South Univ. (2021) 28: 1357−1376

of ball and screw in the x_s direction calculated by combining Eqs. (12a) and (13a).

$$
\begin{aligned}
v_{b-s}^{xs} = &\{r(\delta_{si} - r)(\omega_n \cos\theta_s + \omega_b \sin\theta_s) + \\
&\omega r R_{bs}[(r - \delta_{si})\cos\theta_s - R]\}/2
\end{aligned} \tag{51}
$$

By combining Eqs. (49)−(51), Eq. (48) was deduced as:

$$
h_{rbs}^{xs} = h_{rbs}^{xs}(t_A^{xs}) + \int_{l_A^{xs}}^{l_C^{xs}} k_{bs} \frac{F_{si}}{A(\varsigma_{xs})} v_{rbs}^{xs} \frac{dl_{xs}}{v_{b-s}^{xs}} \tag{52}
$$

In Figure 5, at contact point A_{xs}, $l_A^{xs} = 0$, and at contact point C_{xs}, $l_C^{xs} = 2a_{xs}$.

By considering the rolling cycles number, h_{rbs}^{xs} is expressed as:

$$
h_{rbs}^{xs}(n) = h_{rbs}^{xs}(n-1) + \int_{l_A^{xs}(n)}^{l_C^{xs}(n)} k_{bs} \frac{F_{si}}{A(\varsigma_{xs})} v_{rbs}^{xs}(n) \frac{dl_{xs}}{v_{b-s}^{xs}} \tag{53}
$$

Similarly, the rolling wear depth in the y_s direction can be obtained:

$$
h_{rbs}^{ys}(n) = h_{rbs}^{ys}(n-1) + \int_{l_A^{ys}(n)}^{l_C^{ys}(n)} k_{bs} \frac{F_{si}}{A(\varsigma_{ys})} v_{rbs}^{ys}(n) \frac{dl_{ys}}{v_{b-s}^{ys}} \tag{54}
$$

The term v_{rbs}^{ys} is the sliding velocity between ball and screw in the y_s direction, given by

$$
v_{rbs}^{ys} = v_{b-s}^{ys} \varsigma_{ys} \tag{55}
$$

where v_{b-s}^{ys} is the average rolling velocity of ball and screw in the y_s direction calculated by combining Eqs. (12b) and (13b) as:

$$
v_{b-s}^{ys} = \frac{r(\delta_{si} - r)\omega_t}{2} \tag{56}
$$

Similarly, the cumulative rolling wear depth of ball and nut in the x_n and y_n direction is obtained:

$$
h_{rbn}^{xn} = h_{rbn}^{xn}(t_A^{xn}) + \int_{t_A^{xn}}^{t_i^{xn}} k_{bn} \frac{F_{ni}}{A(\varsigma_{xn})} v_{rbn}^{xn} dt_i^{xn}, \ t_i^{xn} < t_C^{xn} \tag{57a}
$$

$$
h_{rbn}^{yn} = h_{rbn}^{yn}(t_A^{yn}) + \int_{t_A^{yn}}^{t_i^{yn}} k_{bn} \frac{F_{ni}}{A(\varsigma_{yn})} v_{rbn}^{yn} dt_i^{yn}, \ t_i^{yn} < t_C^{yn} \tag{57b}
$$

The sliding velocities of ball and nut in the x_n and y_n direction, i.e., v_{rbn}^{xn} and v_{rbn}^{yn} in Eqs. (57a) and (57b), can be calculated:

$$
v_{rbn}^{xn} = v_{b-n}^{xn} \varsigma_{xn} \tag{58a}
$$

$$
v_{rbn}^{yn} = v_{b-n}^{yn} \varsigma_{yn} \tag{58b}
$$

where ς_{xn} and ς_{yn} are the creep rate of ball and screw in the x_n and y_n directions given by Eqs. (9a) and (9b),

respectively. The terms v_{b-n}^{xn} and v_{b-n}^{yn} are the average rolling velocity of ball and nut in the x_n and y_n directions calculated according to Eqs. (3a), (4a), and Eqs. (3b) and (4b):

$$
\begin{aligned}
v_{b-n}^{xn} = &\{r(\delta_{ni} - r)(\omega_n \cos\theta_n + \omega_b \sin\theta_n) - \\
&\omega_N r R_{bn}[R + (r - \delta_{ni})\cos\theta_n]\}/2
\end{aligned} \tag{59a}
$$

$$
v_{b-n}^{yn} = \frac{r(r - \delta_{ni})\omega_t}{2} \tag{59b}
$$

Considering the rolling cycles number and combining Eqs. (57a) and (57b), h_{rbn}^{xn} and h_{rbn}^{yn} are given by Eqs. (60a) and (60b), respectively:

$$
h_{rbn}^{xn}(n) = h_{rbn}^{xn}(n-1) + \int_{l_A^{xn}(n)}^{l_C^{xn}(n)} k_{bn} \frac{F_{ni}}{A(\varsigma_{xn})} v_{rbn}^{xn}(n) \frac{dl_{xn}}{v_{b-n}^{xn}} \tag{60a}
$$

$$
h_{rbn}^{yn}(n) = h_{rbn}^{yn}(n-1) + \int_{l_A^{yn}(n)}^{l_C^{yn}(n)} k_{bn} \frac{F_{ni}}{A(\varsigma_{yn})} v_{rbn}^{yn}(n) \frac{dl_{yn}}{v_{b-n}^{yn}} \tag{60b}
$$

where $h_{rbs}^{xs}(n-1)$ and $h_{rbs}^{xs}(n-1)$ are the rolling wear depths of ball and nut in the x_n and y_n directions, respectively, when the number of the ball rolling cycles is $(n-1)$. In Figure 5, at contact point A_{xn}, $l_A^{xn} = 0$; at contact point C_{xn}, $l_C^{xn} = 2a_{xn}$. At contact point A_{yn}, $l_A^{yn} = 0$, and at contact point C_{yn}, $l_C^{yn} = 2a_{yn}$.

5 Analysis of BSM precision loss

5.1 Working conditions on precision loss

Figure 6 shows the flowchart of the whole calculation process. When the ball is at different phase angles, the creep rate between ball and screw/nuts varies with the operating conditions (i.e., axial loading and rotational speed). The BSM lead and raceway curvature ratios were obtained from Table 1. The variation of the creep rate with the axial loading can be investigated based on the creep calculation presented in Section 2; the rotational speed of the screw was set to 60 r/min, and the initial preload was set to 2500 N. Besides, the law of the BSM creep rate can be obtained considering the different axial loading conditions in Figures 7(a)−(d). Similarly, the BSM lead was 20 mm, and the raceway curvature ratio was 0.2725 based on Table 1. When the axial loading was set to 2000 N, and the initial preload was 2500 N, the creep rate was obtained considering the different rotational speeds
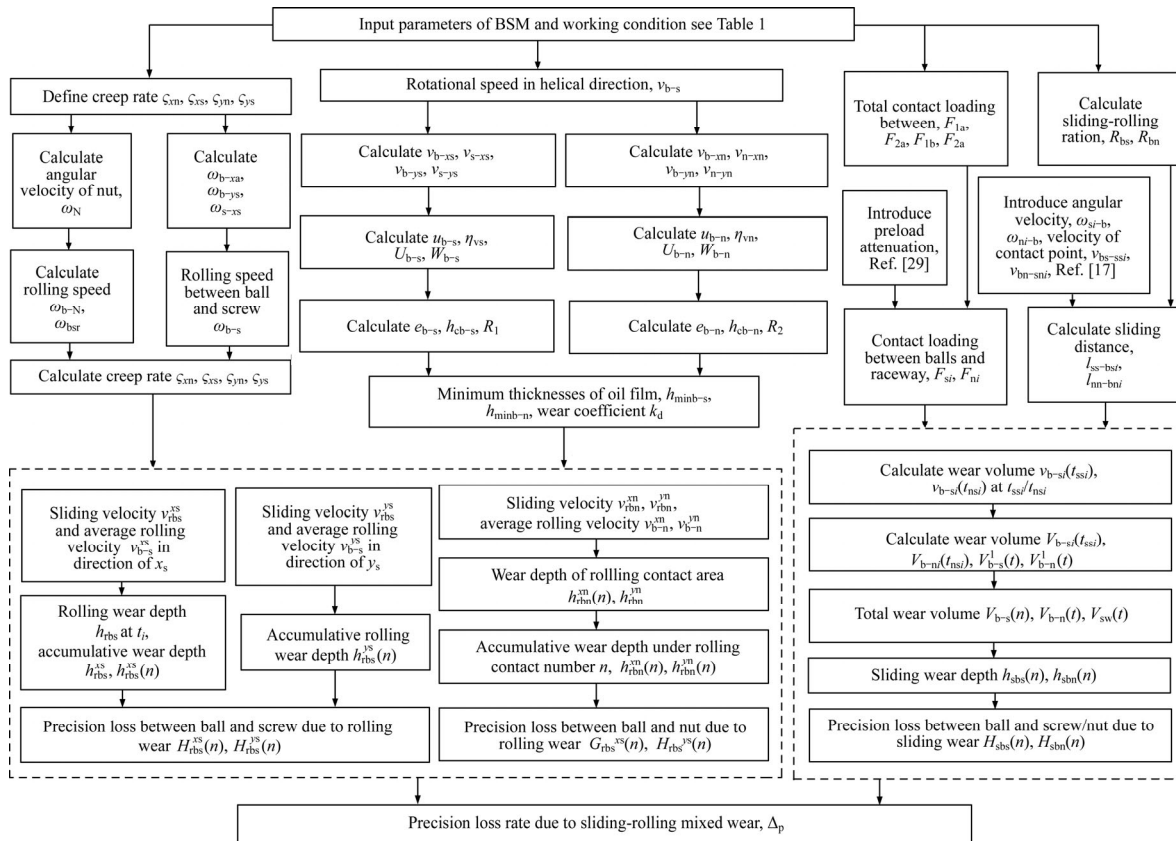
Figure 6 Flowchart of calculation process for BSM precision loss and precision loss rate

in Figures 7(e)−(h).

In Figures 7(a) and (b), the changing characteristics of the creep rate between the ball and the screw raceway are consistent with those of the contact angle. That is, the creep rate between the ball and the screw raceway decreases with reducing contact angle. Also, the creep rate decreases with the increase of the axial load. However, the contact angle θ_n between the ball and the nut raceway increases as the axial load increases. Therefore, in Figures 7(c) and (d), the changing characteristics of the creep rate between the ball and the nut raceway are also consistent with the changing characteristics of the contact angle. That is, the absolute value of the creep rate between the ball and the nut increases as the contact angle increases, and it became more significant as the axial load increases.

In Figures 7(e)−(h), because of the ball spin angular velocity, the rolling speed between ball and screw/nut relates to the contact angle. When the rotational speed of the screw increases, the contact angle θ_s becomes larger. Therefore, in Figures 7(e) and (f), the changing characteristics of the creep rate between the ball and the screw

raceway are consistent with the changing characteristics of the contact angle. That is, the creep rate between the ball and the screw enlarges as the contact angle increases. The performance result was that the creep rate increased with the increase of the screw rotation speed. However, the contact angle θ_n becomes small as the screw rotation speed increases. Therefore, in Figures 7(g) and (h), the changing characteristics of the creep rate between the ball and the nut raceway are also consistent with those of the contact angle. That is, the absolute value of the creep rate between the ball and the screw becomes smaller as the contact angle decreases. Also, as the screw rotation speed increases, the creep rate reduces.

Using KOC301 lubricant, the lubricant viscosities η_{vs} and η_{vn} can be calculated from Eqs. 24(a) and (b). According to Figures 8(a) and (b), both the rotational speed and the axial loading have certain influences on the minimum lubricant film thickness between ball and screw/nut. However, the influence of the rotational speed is more significant than that of the axial loading. Also, the minimum film thickness between the ball and nut is slightly larger than that between ball and screw, because with
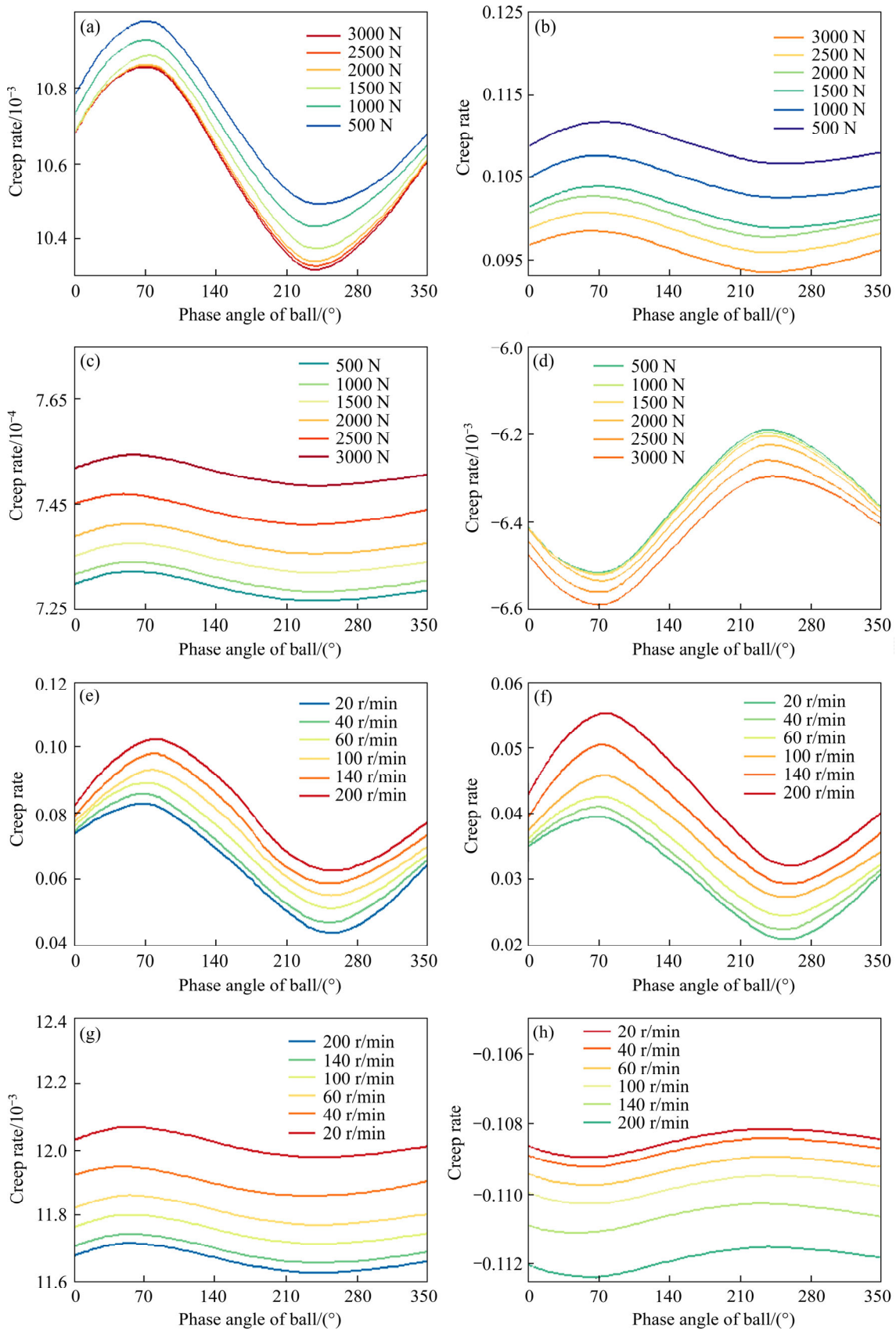
Figure 7 BSM creep rates under rolling contact considering different axial loading conditions (a, b, c, d) and rotational speed conditions (e, f, g, h): (a, e) Ball and screw in x_s direction; (b, f) Ball and screw in y_s direction; (c, g) Ball and nut in x_n direction; (d, h) Ball and nut in y_n direction rates under rolling contact considering different rotational speed conditions
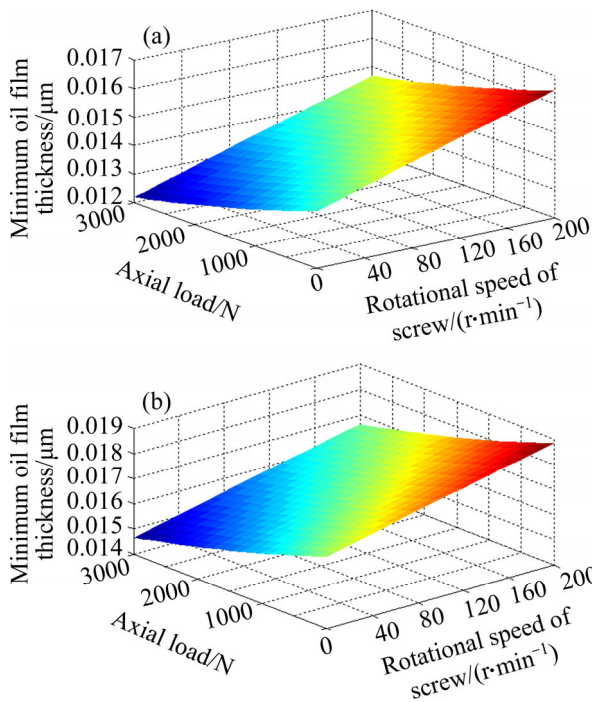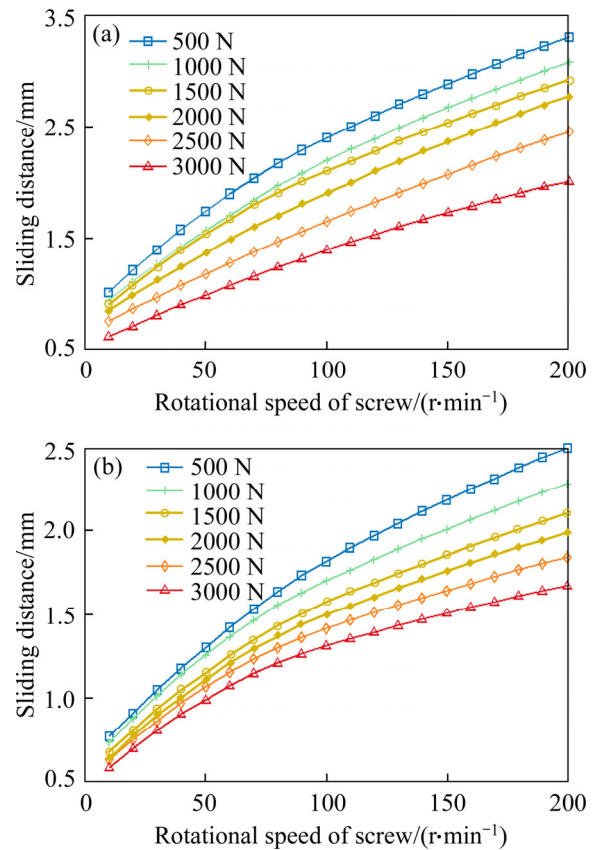
Figure 8 BSM minimum lubricant film thickness under different rotational speed and axial loading working conditions: (a) Minimum lubricant thickness between ball and screw; (b) Minimum lubricant thickness between ball and nut

Figure 9 BSM sliding distance at different rotational speed and axial loading working conditions: (a) Sliding distance between ball and screw; (b) Sliding distance between ball and nut

the increase of the rotational speed and centrifugal force, the minimum lubricant thickness between ball and nut was increased more than that between ball and screw. As the axial loading increases, the contact loading of the ball and screw/nut also increases. Therefore, the minimum lubricant film thickness of the ball and screw/nut reduces.

In this study, when the ball moved from the ith ball position to the $(i+1)$th ball position, the sliding length of screw/nut relative to the original contact point is called the sliding distance. Axial loading and rotational speed have different degrees of influence on the sliding distance. When the initial preload was 2500 N, by combining Eqs. (39a)−(41), the sliding distance of ball and screw/nut is obtained (see Figure 9) considering the effects of axial loading and rotational speed.

According to Figure 9, both the axial loading and rotational speed of the screw have different degrees of influence on the BSM sliding distance. However, compared to the effect of axial loading on the sliding distance, the effect of the rotational speed is more significant. Also, the sliding distance on the screw is greater than that on the nut. The reason for

this phenomenon is the transmission principle of BSM; that is, the movement of the screw drives the ball, and in turn, drives the nut to move. When a sliding movement exists between the ball and the screw raceway, it directly affects the movement between the ball and nut. It causes sliding-to-rolling ratio R_{bs} between the ball and the screw greater than the R_{bn} between ball and nut. Therefore, the sliding distance between the ball and screw is more significant than that between the ball and nut.

5.2 Experimental tests for evaluating precision loss

According to Refs. [6, 20−22], the cumulative wear depth in the stroke direction corresponds to the BSM precision loss value. By combining Eqs. (42a) and (43), the BSM precision degradation owing to the accumulated sliding motion wear depth of ball and screw/nut can be obtained:

$$H_{sbs}(n_1) = \frac{\cos\alpha}{\sin\theta_s}\int_0^{L_{b-s}} h_{sbs}(n_1)\,\mathrm{d}L \qquad (61a)$$

$$H_{\text{sbn}}(n_2) = \frac{\cos\alpha}{\sin\theta_n} \int_0^{L_{\text{b-n}}} h_{\text{sbn}}(n_2)\,\mathrm{d}L \qquad (61\text{b})$$

Compared with WEI's [6], ZHOU's [20], and LIU's [21] models, the BSM precision loss due to sliding motion wear of ball and screw was obtained. Based on Eq. 61(b), the precision loss due to the accumulated sliding motion wear between ball and nut in the stroke direction can also be gained. Figure 10 shows the BSM precision loss due to sliding motion wear.
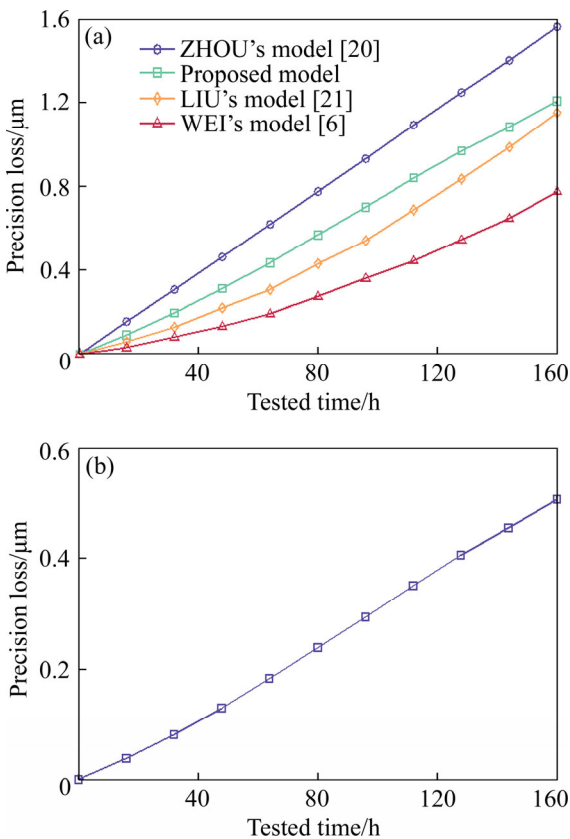
Figure 10 BSM precision loss due to sliding motion wear: (a) Precision loss due to sliding motion wear between ball and screw; (b) Precision loss due to sliding motion wear between ball and nut

By combining Eqs. (9), (15) and (22), the BSM creep rate can be calculated considering the operating conditions. The BSM creep characteristics were obtained at different axial loadings (see Figures 7(a)−(d)) and at different rotational speeds (Figures 7(e)−(h)). Based on Eqs. (47)−(52), the rolling motion wear depth of single ball and screw was obtained. Then, according to Eq. (53), the accumulated rolling motion wear depth of all effective transmission balls and screw in the x_s direction is given by Eq. (62).

$$H_{\text{rbs}}^{xs}(n_1) = M\frac{\cos\alpha}{\sin\theta_s} \int_0^{L_{\text{b-s}}} h_{\text{rbs}}^{xs}(n_1)\,\mathrm{d}L \qquad (62)$$

Similarly, according to Eq. (54), the accumulated rolling motion wear depth of all effective transmission balls and screw in the y_s direction was also obtained:

$$H_{\text{rbs}}^{ys}(n_1) = M\frac{\cos\alpha}{\sin\theta_s} \int_0^{L_{\text{b-s}}} h_{\text{rbs}}^{ys}(n_1)\,\mathrm{d}L \qquad (63)$$

Figure 11(a) shows the variation trend of BSM cumulative rolling motion wear depth obtained by combining Eqs. (62) and (63). Similarly, according to Eqs. (60a) and (60b), the cumulated rolling motion wear depth of all effective transmission balls and nut in the x_n and y_n directions can be written by Eq. (64), and Figure 11(b) shows its variation law.
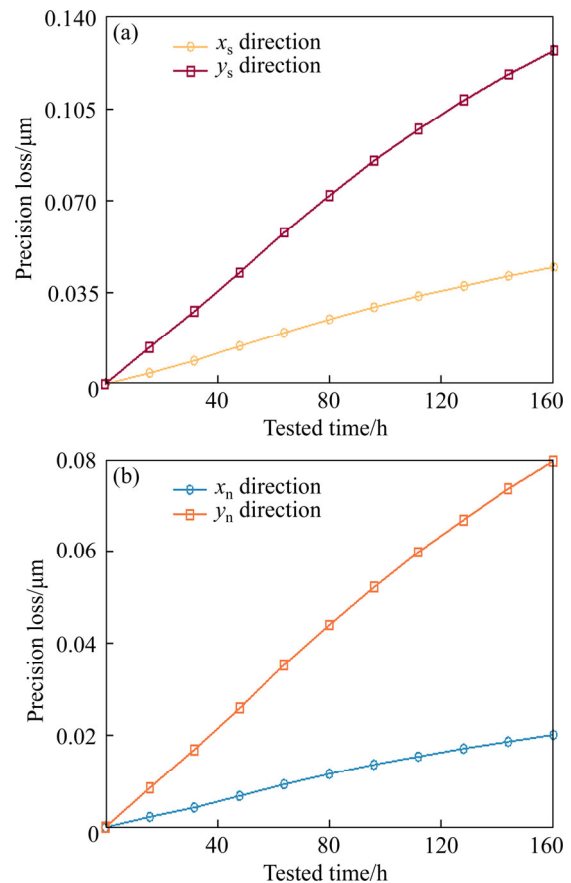
Figure 11 BSM precision loss due to rolling motion wear: (a) Between ball and screw; (b) Between ball and nut

Similarly, according to Eqs. (61), the accumulated wear depth of all effective transmission balls and nut in x_n/y_n direction can be written as follows:

$$H_{\text{rbn}}^{xn}(n_2) = M\frac{\cos\alpha}{\sin\theta_n} \int_0^{L_{\text{b-n}}} h_{\text{rbn}}^{xn}(n_2)\,\mathrm{d}L \qquad (64\text{a})$$

$$H_{\text{rbn}}^{yn}(n_2) = M \frac{\cos\alpha}{\sin\theta_n} \int_0^{L_{\text{b−n}}} h_{\text{rbn}}^{yn}(n_2)\,\mathrm{d}L \qquad (64b)$$

In order to obtain the amount of precision loss when the BSM runs in a stable operating state, the BSM after fully running-in was selected as the experimental object. The positioning error after running was taken as the initial precision value. The experiments were performed using a test platform and a laser interferometer (XD Dual Frequency Laser Interferometer).

The positioning precision of the BSM after the wear test was measured. The difference between the test value and the initial value was the precision loss due to sliding-rolling mixed motion behavior. The following experimental conditions were established: axial loading of 2000 N, rotational speed of 60 r/min, grease-type lubrication using KOC301 lubricant, ambient temperature of 23 °C, test overall duration of 160 h. By combining Eq. (61a) with Eq. (64b), the test process and test results due to sliding-rolling mixed motion were obtained (see Figure 12).
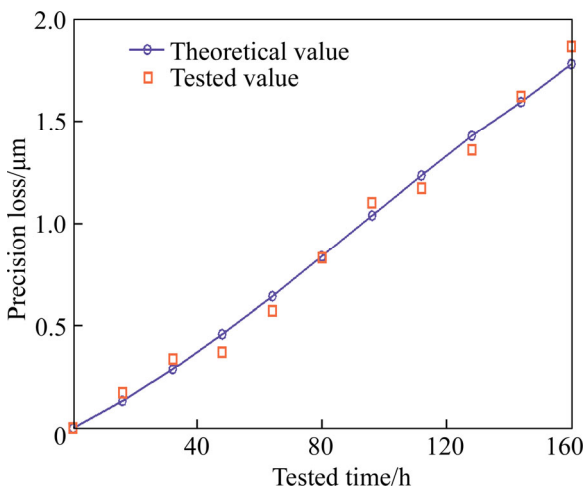
Figure 12 BSM precision loss due to sliding-rolling mixed motion behavior

ZHOU et al [20] and LIU et al [21] established the BSM precision loss model due to screw sliding motion, mainly focusing on screw precision degradation. However, since the screw, nut and ball have different degrees of precision degradation, this study focuses on the BSM precision degradation due to sliding-rolling mixed motion behavior. According to Refs. [20, 21] and combining Eqs. (61a)−(64b), the BSM precision degradation, and precision loss rate were obtained in Eq. (65). Figure 13 shows the
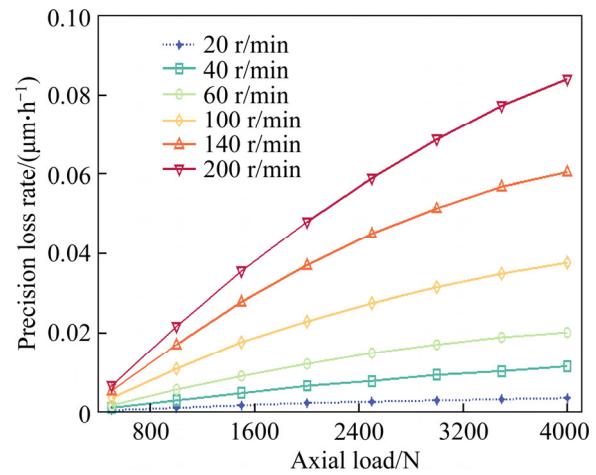
Figure 13 Total precision loss rate of BSM due to sliding-rolling mixed motion behavior

total precision loss rate for the BSM.

$$\begin{cases} \Delta p = Mk_{\text{d}}F_{\text{m}}\tan\alpha\left(\dfrac{rw_{si-\text{b}}}{H_{\text{b−s}}a_k L_s \sin\theta_s} + \dfrac{rw_{ni-\text{b}}}{H_{\text{b−n}}a_k L_n \sin\theta_n}\right)t + \dfrac{9M(k_{\text{bs}}F_{si}v_{\text{rbs}} + k_{\text{bn}}F_{ni}v_{\text{rbn}})}{a_k b_k}t \\[4mm] \Delta p' = Mk_{\text{d}}F_{\text{m}}\tan\alpha\left(\dfrac{rw_{si-\text{b}}}{H_{\text{b−s}}a_k L_s \sin\theta_s} + \dfrac{rw_{ni-\text{b}}}{H_{\text{b−n}}a_k L_n \sin\theta_n}\right) + \dfrac{9M(k_{\text{bs}}F_{si}v_{\text{rbs}} + k_{\text{bn}}F_{ni}v_{\text{rbn}})}{a_k b_k} \end{cases}$$

$$(65)$$

In Figure 13, both the axial loading and rotational speed have different degrees of impact on the BSM precision loss rate. Therefore, a quantitative analysis of the influence degree of axial load and rotational speed on the BSM precision loss rate is required. At a given screw speed, this study uses the variation of the precision loss rate and the variation rate of the precision loss rate to analyze the influence degree of axial load conditions on the precision loss rate. Table 2 summarizes the calculation results. In order to facilitate the quantitative analysis, the accuracy loss rate under an axial load of 500 N was used as a reference.

When analyzing the influence degree of the rotation speed on the accuracy loss rate, it was more reasonable to use the variation rate of the precision loss rate as the quantitative analysis index since the increase rate of the screw rotation speed was different. The variation of the precision loss rate was an intermediate value for calculating the variation rate of the precision loss rate, and it was also

essential. In order to facilitate the quantitative analysis, the precision loss rate at a rotational speed of 20 r/min was used as a reference point. Note that due to the different increase in the screw rotation speed, that is, when the increment of the rotation speed was 40 or 60 r/min, it was necessary to divide by the multiple (2 or 3) of the rotation speed increment when calculating the variation rate of the precision loss rate. After that, the criteria for the unified quantitative analysis can be obtained (Table 3).

From Figure 13 and Table 2, at a given rotational speed, the precision loss rate increases with the increase of axial load. However, when the axial load increases by the same amplitude, the variation (increased amount) of the precision loss rate gradually decreases, and the variation rate of precision loss rate gradually decreases. The reason is that as the axial load increases, the contact angle between the ball and the screw decreases. As a result, the contact load between the ball and screw enlarges, and so does the precision loss rate between the ball and screw. However, the contact angle between the ball and the nut increases so that the contact load between the ball and the nut becomes smaller, resulting in the precision loss rate between the ball and nut also becoming smaller. Therefore, when the axial load increases, although the precision loss rate enlarges, the change value (increased amount) of the total precision loss rate of the ball screw decreases, and the variation rate of the precision loss rate gradually decreases.

At a given screw rotation speed, the increase in the precision loss rate is the maximum when the axial load changes from 500 to 1000 N. Moreover, the variation rate (increase rate) of the accuracy loss rate also reaches the maximum at 1000 N axial load. As the axial load increases, the amplitudes of attenuation of the variation value and the variation rate of the BSM precision loss are different. In particular, through the variation rate of precision loss rate, it is more convenient to analyze the change law of precision loss rate quantitatively.

According to the analysis of Figure 13 and Table 3, at a given axial load, the precision loss rate enlarges as the screw rotation speed increases. However, as the rotation speed gradually increases, the increase rate of the precision loss rate gradually decreases. On the one hand, due to the increase in rotation speed, the sliding motion velocity becomes more significant and so does the sliding motion distance (Eq. (39) and Figure 9), resulting in the accelerated sliding motion wear, and the increased precision loss and precision loss rate. On the other hand, as the rotational speed of the screw increases, the contact angle between the ball and the nut decreases. The contact load between the ball and the nut increases, increasing the precision loss rate

Table 2 Influence degree of axial load conditions on BSM precision loss rate

Rotational speed/ (r·min⁻¹)	Parameter	Axial load/N							
		500	1000	1500	2000	2500	3000	3500	4000
20	Variation of precision loss rate	0	0.0006975	0.0006103	0.0005231	0.0004359	0.0003487	0.0002616	0.0001744
	Variation rate of precision loss rate/%	0	160.0000	53.8462	30.0001	19.2308	12.9032	8.5714	5.2632
40	Variation of precision loss rate	0	0.002005	0.001831	0.001656	0.001482	0.001308	0.001133	0.0009590
	Variation rate of precision loss rate/%	0	209.0909	61.7647	34.5455	22.9730	16.4835	12.2642	9.2437
60	Variation of precision loss rate	0	0.003923	0.003487	0.003051	0.002616	0.002180	0.001744	0.001308
	Variation rate of precision loss rate/%	0	225.0000	61.5385	33.33333	21.4286	14.7059	10.2564	6.9767
100	Variation of precision loss rate	0	0.007367	0.006800	0.005100	0.004534	0.003967	0.003400	0.002833
	Variation rate of precision loss rate/%	0	216.6667	63.1579	29.0323	20.0000	14.5833	10.9091	8.1967
140	Variation of precision loss rate	0	0.01183	0.01052	0.009203	0.007888	0.006574	0.005259	0.003944
	Variation rate of precision loss rate/%	0	225.0002	61.5385	33.3333	21.4286	14.7059	10.2564	6.9767
200	Variation of precision loss rate	0	0.01505	0.01374	0.01243	0.01112	0.009816	0.008507	0.006544
	Variation rate of precision loss rate/%	0	230.0000	63.6364	35.1852	23.2877	16.6667	12.3810	8.4746

Table 3 Influence degree of rotational speed conditions on BSM precision loss rate

Axial load/N	Parameter	Rotational speed/(r·min⁻¹)					
		20	40	60	100	140	200
500	Variation of precision loss rate	0	0.0005231	0.0007847	0.001656	0.001859	0.001285
	Variation rate of precision loss rate/%	0	120.0001	81.8182	47.5000	27.3333	8.1461
1000	Variation of precision loss rate	0	0.001831	0.002703	0.005100	0.006324	0.004504
	Variation rate of precision loss rate/%	0	161.5385	91.1765	45.0000	29.3684	8.7843
1500	Variation of precision loss rate	0	0.003051	0.004359	0.008413	0.010042	0.007729
	Variation rate of precision loss rate/%	0	175.0000	90.9091	45.9524	28.5806	9.3313
2000	Variation of precision loss rate	0	0.004185	0.005754	0.01046	0.01415	0.01096
	Variation rate of precision loss rate/%	0	184.6154	89.1892	42.8571	31.2000	9.9238
2500	Variation of precision loss rate	0	0.005231	0.006888	0.01238	0.01750	0.01420
	Variation rate of precision loss rate/%	0	193.5484	86.8132	41.7647	32.1667	10.5861
3000	Variation of precision loss rate	0	0.006190	0.007759	0.01417	0.02011	0.01744
	Variation rate of precision loss rate/%	0	202.8571	83.9623	41.6667	32.2545	11.3369
3500	Variation of precision loss rate	0	0.007062	0.008370	0.01582	0.02197	0.02069
	Variation rate of precision loss rate/%	0	213.1579	80.6723	42.2093	31.7705	12.1976
4000	Variation of precision loss rate	0	0.007847	0.008718	0.01735	0.02308	0.02329
	Variation rate of precision loss rate/%	0	225.0000	76.9231	43.2609	30.8485	12.8351

between the ball and nut. However, the contact angle between ball and screw increases, so that the contact load between ball and screw reduces. Also, the precision loss rate between the ball and screw reduces. Therefore, when the rotation speed increases, although the precision loss rate becomes larger, the variation rate (increase rate) of the total precision loss rate of the BSM decreases.

At a given axial load, the variation rate of the precision loss rate reaches its maximum when the screw rotation speed changes from 20 to 40 r/min. When the speed is 40 r/min, as the axial load increases, the increase rate in the precision loss rate gradually becomes larger. Furthermore, at the 4000 N axial load, the increase rate of the precision loss rate is the maximum. As the screw rotation speed increases, the variation value and variation rate of the BSM precision loss rate have different amplitudes of attenuation. Especially through the variation rate of the precision loss rate, it was more convenient to quantitatively analyze the influence degree of the rotation speed on the BSM precision loss rate.

6 Conclusions

1) Under the action of sliding motion, the precision loss value of the screw is greater than that of nut, because the sliding distance between the ball and the screw is greater than that between the ball and the nut. The sliding motion wear depth between ball and screw contributes a large proportion to the BSM precision loss.

2) The precision loss value under rolling motion occupies a certain proportion of the precision loss value under sliding motion, and the precision loss value under rolling motion is a part of the total precision loss of the ball screw. The precision loss value due to rolling motion has a certain level of influence on the BSM total precision loss.

3) As the rotation speed gradually increases, the increase rate of the precision loss rate gradually decreases. The rotation speed had a certain effect on the contact angle and could increase the sliding velocity, resulting in the increase of precision loss rate.

Contributors

QI Bao-bao provided the data curation, methodology and writing-original draft. CHENG Qiang provided the funding acquisition and methodology. LI Shun-lei replied to reviewers' comments and revised the final version. LIU Zhi-feng conducted the formal analysis and funding acquisition. YANG Cong-bin provided the software.

Conflict of interest

QI Bao-bao, CHENG Qiang, LI Shun-lei, LIU Zhi-feng and YANG Cong-bin declare that they have no conflict of interest.

References

[1] YANG Y, ZHANG W M, ZHU Q X, JIANG Q S. Dynamic characteristic optimization of ball screw feed drive in machine tool based on modal extraction of state space model [J]. IEEE Access, 2019, 7: 55524-55542. DOI: 10.1109/ACCESS.2019. 2909550.

[2] LIN M C, RAVANI B, VELINSKY S A. Kinematics of the ball screw mechanism [J]. Journal of Mechanical Design, 1994, 116(3): 849−855. DOI: 10.1115/1.2919459.

[3] WEI C C, LIN J F. Kinematic analysis of the ball screw mechanism considering variable contact angles and elastic deformations [J]. Journal of Mechanical Design, 2003, 125(4): 717−733. DOI: 10.1115/1.1623761.

[4] LIN M C, VELINSKY S A, RAVANI B. Design of the ball screw mechanism for optimal efficiency [J]. Journal of Mechanical Design, 1994, 116(3): 856−861. DOI: 10.1115/ 1.2919460.

[5] LIU H, ZHANG J, ZHAO W. An intelligent non-collocated control strategy for ball-screw feed drives with dynamic variations [J]. Engineering, 2017, 3(5): 641−647. DOI: 10.1016/J.ENG.2017.04.007.

[6] WEI C, LAI R. Kinematical analyses and transmission efficiency of a preloaded ball screw operating at high rotational speeds [J]. Mechanism and Machine Theory, 2011, 46(7): 880−898. DOI: 10.1016/j.mechmachtheory.2011. 02.009.

[7] WEI C C, LIN J F, HORNG J. Analysis of a ball screw with a preload and lubrication [J]. Tribology International, 2009, 42: 11−19. DOI: 10.1016/j.triboint. 2008.12.013.

[8] CHEN Yong-jiang, TANG Wen-cheng. Dynamic contact stiffness analysis of a double-nut ball screw based on quasi-static method [J]. Mechanism and Machine Theory, 2014, 73(3): 76−90. DOI: 10.1016/j.mechmachtheory.2013. 10.008.

[9] ZHAO J, LIN M, SONG X, GUO Q Z. Investigation of load distribution and deformations for ball screws with the effects of turning torque and geometric errors [J]. Mechanism and Machine Theory, 2019, 141: 95−116. DOI: 10.1016/ j.mechmachtheory.2019.07.006.

[10] ZHEN N, AN Q. Analysis of stress and fatigue life of ball screw with considering the dimension errors of balls [J]. International Journal of Mechanical Sciences, 2018, 137: 68−76. DOI: 10.1016/j.ijmecsci.2017.12. 038.

[11] LIN B, OKWUDIRE C E, WOU J S. Low order static load distribution model for ball screw mechanisms including effects of lateral deformation and geometric errors [J]. Journal of Mechanical Design, 2018, 140(2): 022301. DOI: 10.1115/ 1.4038071.

[12] KANG X M, WANG L. Experimental analysis of axial load internal circulation ball screw pair of friction torque and the impact [J]. Applied Mechanics and Materials, 2013, (401−403): 139−145. DOI: 10.4028/www.scientific.net/ AMM.401-403.139.

[13] XU N, TANG W, CHEN Y, BAO D, GUO Y. Modeling analysis and experimental study for the friction of a ball screw [J]. Mechanism and Machine Theory, 2015, 87: 57−69. DOI: 10.1016/j.mechmachtheory. 2014.12.019.

[14] ZHOU C, FENG H, CHEN Z, OU Y. Correlation between preload and no-load drag torque of ball screws [J]. International Journal of Machine Tools & Manufacture, 2016, 102: 35−40. DOI: 10.1016/j. ijmachtools.2015.11.010.

[15] WEI C C, LIOU W L, LAI R S. Wear analysis of the offset type preloaded ball-screw operating at high speed [J]. Wear, 2012, 292: 111−123. DOI: 10.1016/j.wear. 2012.05.024.

[16] KAMALZADEH A, GORDON D J, ERKORKMAZ K. Robust compensation of elastic deformations in ball screw drives [J]. International Journal of Machine Tools & Manufacture, 2010, 50(6): 559−574. DOI: 10.1016/ j.ijmachtools.2010.03.001.

[17] GNANAMOORTHY R, GOVINDARAIAN N, MUTOH Y. Effect of slid-roll ratio on the contact fatigue behavior of sintered and hardened steels [J]. Journal of Failure Analysis and Prevention, 2004, 4(2): 78−83. DOI: 10.1361/ 15477020419082.

[18] GOVINDARAJAN N, GNANAMOORTHY R. Rolling/ sliding contact fatigue life prediction of sintered and hardened steels [J]. Wear, 2007, 262(1, 2): 70−78. DOI: 10.1016/ j.wear.2006.03.053.

[19] ARCHARD J F. Contact and rubbing of flat surfaces [J]. Journal of Applied Physics, 1953, 24(8): 981−988. DOI: 10.1063/1.1721448.

[20] ZHOU C, OU Y, FENG H, CHE Z. Investigation of the precision loss for ball screw based on the modified Archard theory [J]. Industrial Lubrication and Tribology, 2017, 69(2): 166−173. DOI: 10.1108/ILT-12-2015-0204.

[21] LIU Jia-lan, CHI Ma, WANG Shi-long. Precision loss modeling method of ball screw pair [J]. Mechanical Systems and Signal Processing, 2020, 135: 106397. DOI: 10.1016/ j.ymssp.2019.106397.

[22] CHENG Q, QI BB, LIU Z F, ZHANG C X, XUE D Y. An accuracy degradation analysis of ball screw mechanism considering time-varying motion and loading working conditions [J]. Mechanism and Machine Theory, 2019, 134: 1−23. DOI: 10.1016/ j.mechmachtheory. 2018.12.024.

[23] ZHOU C G, ZHOU H X, FENG H T. Experimental analysis of the wear coefficient of double-nut ball screws [J]. Wear, 2020, 446: 203201. DOI: 10.1016/j. wear.2020.203201.

[24] LIU K, LIU H, LI T, WANG Y, SUN M, WU Y. Prediction of comprehensive thermal error of a preloaded ball screw on a gantry milling machine [J]. Journal of Manufacturing Science and Engineering, 2017, 140(2): 021004. DOI: 10.1115/1.4037236.

[25] NGUYEN T L, RO S K, PARK J W. Study of ball screw system preload monitoring during operation based on the motor current and screw-nut vibration [J]. Mechanical Systems and Signal Processing, 2019, 131: 18−32. DOI: 10.1016/j.ymssp.2019.05.036.

[26] CHENG Q, ZHAO H W, ZHAO Y S, SUN B W, GU P H. Machining accuracy reliability analysis of multi-axis machine tool based on Monte Carlo simulation [J]. Journal of Intelligent Manufacturing, 2018, 29(1): 191−209. DOI: 10.1007/s10845-015-1101-1.

[27] CAI L G, ZHANG Z L, CHENG Q, LIU Z F, GU P H. An approach to optimize the machining accuracy retainability of multi-axis NC machine tool based on robust design [J]. Precision Engineering, 2016, 43: 370−386. DOI: 10.1016/j.precisioneng.2015.09.001.

[28] CHENG Q, FENG Q N, LIU Z F, GU P H, ZHANG G J. Sensitivity analysis of machining accuracy of multi-axis machine tool based on POE screw theory and Morris method [J]. The International Journal of Advanced Manufacturing Technology, 2016, 84(9−12): 2301−2318. DOI: 10.1007/s00170-015-7791-x.

[29] CHENG Q, ZHAO H W, ZHANG G G, GU P H, CAI L G. An analytical approach for crucial geometric errors identification of multi-axis machine tool based on global sensitivity analysis [J]. International Journal of Advanced Manufacturing Technology, 2014(75): 107−121. DOI: 10.1007/s00170-014-6133-8.

[30] ZHANG Z L, CAI L G, CHENG Q, LIU Z F, GU P H. A geometric error budget method to improve machining accuracy reliability of multi-axis machine tools [J]. Journal of Intelligent Manufacturing, 2019, 30(2): 495−519. DOI: 10.1007/ s10845-016-1260-8.

[31] FAN J W, TAO H H, WU C J, PAN R, TANG Y H, LI Z S. Kinematic errors prediction for multi-axis machine tools' guideways based on tolerance [J]. The International Journal of Advanced Manufacturing Technology, 2018, 98(5−8): 1131−1144. DOI: 10.1007/s00170-018-2335-9.

[32] RODRÍGUEZ-TEMBLEQUE L, ABASCAL R, ALIABADI M H. A boundary element formulation for wear modeling on 3D contact and rolling-contact problems [J]. International Journal of Solids and Structures, 2010, 47(18, 19): 2600−2612. DOI: 10.1016/j.ijsolstr. 2010.05.021.

[33] KALKER J J, JOHNSON K L. Three-dimensional elastic bodies in rolling contact [J]. Journal of Applied Mechanics, 1993, 60(1): 34−45. DOI: 10.1007/978-94-015-7889-9.

[34] HOU K P, ZHU D, WEN S Z. An inverse solution to the point contact EHL problem under heavy load [J]. ASME Journal of Tribology, 1987, 109(3): 432−436. DOI: 10.1115/1.3261466.

[35] HAMROCK B J, DOWSON D. Isothermal elastohydrodynamic lubrication of point contacts: Part 3−Fully flooded results [J]. Journal of Lubrication Technology, Trans ASME, 1977, 99(2): 264−276. DOI: 10.1115/ 1.3453074.

[36] DING H, KAHRAMAN A. Interactions between nonlinear spur gear dynamics and surface wear [J]. Journal of Sound and Vibration, 2007, 307(3−5): 662−679. DOI: 10.1016/j.jsv.2007.06.030.

[37] MARKHO P H. Highly accurate formulas for rapid calculation of the key geometrical parameters of elliptic Hertzian contacts [J]. ASME Journal of Tribology, 1988, 109(4): 640−647. DOI: 10.1115/ 1.3261525.

[38] LAUN H M. Pressure dependent viscosity and dissipative heating in capillary rheometry of polymer melts [J]. Rheologica Acta, 2003, 42(4): 295−308. DOI: 10.1007/ s00397-002-0291-6.

[39] SHIMIZU S, SHIMODA H, SHARMA C S. Re-evaluation of basic dynamic load rating and life formula for a ball screw [J]. Tribology Transactions, 2007, 50(1): 88−95. DOI: 10.1080/ 104020006011 05599.

[40] MEI X, TSUTSUMI M, TAO T, SUN N. Study on the load distribution of ball screws with errors [J]. Mechanism and Machine Theory, 2003, 38(11): 1257−1269. DOI: 10.1016/ S0094-114X(03)00070-3.

[41] VERL A, FREY S, HEINZE T. Double nut ball screw with improved operating characteristics[J]. CIRP Annals-Manufacturing Technology, 2014, 63(1): 361-364. DOI: 10.1016/j.cirp.2014.03.128.

[42] CHEN K, ZU L, WANG L. Prediction of preload attenuation of ball screw based on support vector machine [J]. Advances in Mechanical Engineering, 2018, 10(9): 1687814018799161. DOI: 10.1177/1687814018799161.

(Edited by FANG Jing-hua)

中文导读

滑-滚混合运动行为作用下的滚珠丝杠副精度损失

摘要：滑-滚混合运动行为在不同程度上会退化滚珠丝杠副的精度。基于滚珠与丝杠/螺母滚道之间的滑-滚混合运动分析，研究了滚珠丝杠副在不同轴向负载及旋转速度工况下的精度损失。由于滑动、滚动磨损与蠕滑、润滑紧密相关，研究了不同运行工况下蠕滑及润滑特性。此外，当探究滚珠与滚道之间的滑动运动行为对精度损失的影响时，计算了滚珠丝杠副的精度损失并对比了其他模型。最后，在给定运行工况下，研究了滑-滚混合运动下的精度损失，设计相关实验，对精度衰退模型进行验证。精度损失的分析结果与试验测试具有很好的吻合性，表明该模型能够很好地预测处于稳定磨损时期内的精度损失。

关键词：滚珠丝杠副；精度损失；滑-滚混合运动；蠕滑；润滑